Electronic structure and peculiar bonding properties of NdNiMg5 from first principles

Samir F. Matar, Bassem Ourane, Etienne Gaudin, Jean-Louis Bobet, Adel F. Al Alam, Naim N. Ouaini

Accepted with Elsevier (Solid State Sciences) Sept.15 2014

Electronic structure and peculiar bonding properties of $NdNiMg_5$ from first principles.

Samir F. Matar[1,*], Bassem Ourane[1], Etienne Gaudin[1], Jean-Louis Bobet[1], Adel F. Al Alam[2], Naïm Ouaini[2].

[1]CNRS, Université de Bordeaux, ICMCB. 33600 Pessac. France.

[2]Université Saint Esprit de Kaslik, CSR-USEK, CNRS_L, Jounieh, Liban.

*Corresponding author: matar@icmcb-bordeaux.cnrs.fr ; abouliess@gmail.com

Keywords: Intermetallics. Magnetism. DFT. Cohesive energy. Elastic properties. Chemical bonding.

Dedication: This work is dedicated to Professor René Otayek.

Abstract:

The newly found ternary compound $NdNiMg_5$ has been studied within DFT based methodologies. Results of cohesive energy, charge transfers, elastic constants and electron localized function mapping as well as electronic structure and bonding properties have been compared with those of isostructural binary NdNi. The calculation results have shown that Mg substructures interlayering *NdNi*–like slabs exhibit different magnitudes of charge transfers all within range of metallic behavior and the different Mg sublattices structures selectively bind with Nd and Ni substructures. As a consequence an enhanced cohesion with respect to binary intermetallic NdNi is identified. The whole set of elastic constants and their combinations in orthorhombic symmetry confirm the mechanical stability of $NdNiMg_5$ with larger compressibility and less ductility (more brittleness) with respect to NdNi. While in an intermetallic compound such as NdNi the bonding is ensured by Nd-Ni interaction, in $NdNiMg_5$ Nd-Ni, Nd-Mg, Ni-Mg as well as Mg-Mg participate to the bonding and the extra electrons brought by Mg are found within bonding states thus illustrating furthermore the enhanced cohesion of the ternary versus the binary systems.

1. Introduction

Magnesium rich compounds are of interest in the field of materials science for crystal chemistry fundamentals [1,2] and for different applications such as corrosion resistance compounds within the Mg-Zn-RE ternary (RE: Rare Earth) [3] and host compounds for hydrogen storage in the solid state [4,5]. The ternary compound $LaCuMg_4$ can be considered from the crystal chemistry point of view as Mg inserted LaCuMg [6]. While exploring the Mg rich side of Mg-Nd-Ni ternary phase diagram Ourane *et al.* discovered the Mg rich ternary $NdNiMg_5$ [7] characterized by a new unusual structure and a long range antiferromagnetic order. Whereas the ternary NdNiMg does not exist, i.e. oppositely to the LaCuMg ternary, $NdNiMg_5$ can be structurally described as Mg inserted NdNi intermetallic with interpenetrating networks of Mg and largely separated NdNi ($c/2$ ~6.9 Å). This can be visualized in a projection of the structure given in Fig. 1 stressing the succession of NdNi and Mg layers along the long orthorhombic *c* axis. Also the base centered orthorhombic symmetry with *Cmcm* space group of the intermetallic NdNi is also found in the Mg rich ternary. Mg-Mg distances are in the range of ~3 Å close to the sum of Mg metallic radii so that one may expect metallic like Mg network. Short Mg–Mg connections are found in ternary magnesium-rich compounds within the Ce-Ru-Mg ternary phase diagram as $CeRu_2Mg_5$ and $Ce_2Ru_4Mg_{17}$ compositions [8]. However the schematic view in Fig. 1 of $NdNiMg_5$ merely gives a qualitative description of the structure due to the belonging of magnesium to three different substructures designated in Fig. 1 with different distances to Nd and Ni (cf. Table 1). Consequently the propose of the present work is to provide a quantitative assessment of the electronic and magnetic structures and of the peculiar bonding properties of $NdNiMg_5$ with respect to NdNi within computations carried out in the well established framework of the quantum density functional theory (DFT) [9,10].

2. Computational details

Two computational methods within the DFT were used in a complementary manner. The Vienna ab initio simulation package (VASP) code [11,12] allows geometry optimization, charge transfer trends and cohesive energy calculations. For this we use the projector augmented wave (PAW) method [13], with the generalized gradient approximation (GGA) scheme following Perdew, Burke and Ernzerhof (PBE) [14].

Semi-core $2p^6$ states were considered upon building the PAW Mg potential. The conjugate-gradient algorithm [15] is used in this computational scheme to relax the atoms. The tetrahedron method with Blöchl corrections [13] as well as a Methfessel-Paxton [16] scheme was applied for both geometry relaxation and total energy calculations. Brillouin-zone (BZ) integrals were approximated using special **k**-point sampling [17]. The optimization of the structural parameters was performed until the forces on the atoms were less than 0.02 eV/Å and all stress components less than 0.003 eV/Å^3. The calculations are converged at an energy cut-off of 400 eV for the plane-wave basis set with respect to the k-point integration up to 12 × 12 × 4 (k_x, k_y, k_z) for best convergence and relaxation to zero strains. The calculations are scalar relativistic. From the calculations, an illustration of the electron distribution is accessed from the electron localization function (ELF) [18]. ELF is a normalized function between 0 (zero localization, blue zones) and 1 (strong localization, red zones) with the value of ½ corresponding to a free electron gas behavior (green zones) –cf. Fig. 2. Also an analysis of the charge density is done with the approach of "atoms in molecules and crystals" (AIM) introduced by Bader [19] whereby molecules are divided into atoms. Following Bader, each atom in the compound is surrounded by a surface running through minima of the charge density. Then the total charge of an atom is determined by integration within the Bader region. Such an analysis can be useful when trends of charge transfer are sought; they do not constitute a tool for evaluating absolute ionizations. In the presently studied compound we evaluate the changes in total charges between title compound $NdNiMg_5$ and the intermetallic NdNi.

Subsequent all-electrons calculations with the GGA were carried out for a full description of the electronic structure and the properties of chemical bonding, using the augmented spherical wave (ASW) method devised by Williams, Kübler and Gelatt in 1979 [20,21] as a linearized method close to LMTO (Linearized Muffin Tin Orbitals). The ASW method has benefited from continuous developments leading to full potential FP-ASW with implementation of chemical bonding according to different schemes (cf. text book by V. Eyert [22] and therein references). The ASW method uses a minimal basis set for the valence states with the outermost shells representing one of each kind: the valence states and the matrix elements are constructed using partial waves up to $l_{max}+1 = 4$ for Nd; $l_{max}+1 = 3$ for Ni and $l_{max}+1 = 2$ for Mg. Self-consistency is achieved when charge transfers and energy changes between two successive cycles were below 10^{-8} and 10^{-6} eV, respectively. BZ integrations were performed using the linear tetrahedron method within the irreducible wedge. Calculation are first carried

out for a non magnetic, spin degenerate configuration (NSP) for assessing the instability of the electronic system towards magnetic polarization and for examining the properties of chemical bonding, then spin polarized (SP) calculations are carried out for two spin channels ↑ and ↓ in an implicit ferromagnetic order (SP-F), with four *f*-electrons for Nd, the 4*f*-subshell is only partially filled. From this, the single particle scheme of the GGA is good enough concerning electronic correlations as shown in Ce-based [23] and Nd based [24] intermetallic compounds. This is with respect to possible improvements with the introduction of a Coulomb on site repulsion parameter within so called GGA+U scheme [25]. Such preliminary calculations were carried out to check this point. They showed only a small departure from the single particle picture, *e.g.* for the lowering of the 4*f* density of states (DOS) at the Fermi level, pushing it down in energy. Lastly for modeling the ground state found antiferromagnetic by experiment [7], SP-AF calculations were done by considering half subcell as "SPIN UP" and the other half as "SPIN DOWN". Besides the site and spin projected density of states, we discuss qualitatively the pair interactions based on the overlap population analysis with the crystal orbital overlap population (COOP) [26]. In the plots, positive, negative, and zero COOP indicate bonding, anti-bonding, and non-bonding interactions, respectively.

3. Geometry optimization results.

Geometry optimization and relative charge transfers.

Starting from the experimental structure parameters of $NdNiMg_5$ [7] and NdNi [27] given in Table 1, unconstrained geometry optimization runs were carried out. In both compounds the orthorhombic symmetry in *Cmcm* space group is preserved after successive calculations with increasing precision of the BZ. As shown in Table 1, the fully relaxed structure parameters are found close to starting ones and the shortest interatomic distances are in agreement with experiment. Especially d(Nd-Ni) is smaller in the ternary and the shortest metal-magnesium connections are for Nd-Mg1 and Ni-Mg2. Mg3 is at large separation from either Nd or Ni. These observations let suggest different charge transfer trends (*Q*) along the different substructure constituents. This can be analyzed from the charge density CHGCAR file obtained from the calculations using the AIM theory [19] introduced above applied to both the ternary and the binary compounds:

$NdNiMg_5$: *Q*(Nd) = +0.51, *Q*(Ni) = –0.98, *Q*(Mg1) = +0.10, *Q*(Mg2) = +0.02 and *Q*(Mg3) ~0.

NdNi: Q(Nd) = +0.63, Q(Ni) = –0.63.

Looking at the binary intermetallic the amount of charge transfer of ±0.63 is small as one would expect in an intermetallic compound. Charge flows from Nd to Ni and this follows the course of the respective electronegativities, larger for Ni versus Nd: χ(Ni) = 1.91; χ(Nd) = 1.14. Its magnitude is significant of a covalent like bonding as one would expect from a metallic compound. In the ternary magnesium rich compound the charge imbalance is changed with a smaller positive charge on Nd and a much larger magnitude negative charge on Ni arising from the presence of neighboring Mg, especially Mg1 which is charged +0.1 whereas Mg2 carries a small charge of +0.02 whereas Mg3 is nearly neutral. Also the smaller charge on Nd as with respect to its value in NdNi, is due to the charge transfer from Mg. Note that χ(Mg) = 1.31 is larger than Nd's but the major change in the Mg rich ternary is observed for Ni.

Electron localization function contours plots.

We illustrate these results with electron localization function ELF shown in Fig. 2 for a slice crossing all constituents labeled with their belonging to the different sub-structures, especially Mg. This projection resembles the sketch of the crystal structure given in Fig. 1. The strong electron localization around Nd arises from the inclusion of core electrons of filled subshells in the construction of the PAW potential. Green areas are found around Ni meaning that its negative charge obtained above is actually signaling a delocalized free electron-like behavior between the atomic constituents; this is also observed between Ni and Nd as well as between Nd and Mg1 with a metallic like bonding. Also the ELF contours extend from Ni to Mg2 (green to yellow) indicating the bonding between them as it is discussed here below with the COOP. Between *NdNi*-like layers the Mg sub-structures show the peculiar behavior of exhibiting strong localization (dark yellow, reddish spots). Mg-Mg metallic bonding is then present as proposed in the introduction and the schematic behavior of a metallic Mg substructure interlayering *NdNi* finds its illustration here.

Cohesive energies.

The question arises as to the role of Mg adjunction/insertion within NdNi in the stability of the binary. This should be quantified from examining the magnitudes of the cohesive energies. $E_{\text{coh.}} = E_{\text{total}}$(compound) - ΣE(constituents). The energies of the constituents were

calculated in their ground state structures. Mg (hexagonal, with $2p^6$ semi-core states): –2.784 eV (2 atoms); Nd (hexagonal): –9.48 eV (2 atoms) and Ni (FCC): -5.51 eV (1 atom). Then $E_{coh.}(NdNiMg_5)$ = –1.59 eV /FU and $E_{coh.}(NdNi)$ = –0.74 eV /FU. This peculiar result translates the large stability provided to the binary intermetallic by Mg through covalent like bonding with Nd as well as Ni.

Elastic constants bulk and shear modules

In orthorhombic symmetry there are nine independent elastic stiffness constants C_{11}, C_{22}, C_{33}, C_{44}, C_{55}, C_{66}, C_{12} C_{23} and C_{13}. Most encountered compounds are polycrystalline with randomly oriented mono-crystalline grains so that on a large scale, such materials can be considered as statistically isotropic. They are then completely described by the bulk modulus *B* and the shear modulus *G*, which may be obtained by averaging the single-crystal elastic constants. The most widely used averaging method of the elastic stiffness constants is Voigt's based on a uniform strain (cf. Ref. [25] for a review). The calculated set of elastic constants in $NiNdMg_5$ and NdNi are given in Table 2. All nine C_{ij} are positive. This condition and the positive magnitudes of C_{ij} combinations pertaining to the stability [28,29] are obeyed. Comparative mechanical properties are obtained from the calculations of the respective bulk and shear modules, B_V and G_V following Voigt and formulated as follows:

$$B_V=1/9\{(C_{11}+C_{22}+C_{33}+C_{33}) + 2(C_{12}+C_{23}+C_{13})\} \text{ and}$$

$$G_V=1/15(C_{11}+C_{22}+C_{33}+C_{33}) – 1/15\ \{(C_{12}+ C_{13}+ C_{23}) – 3(C_{44}+C_{55}+2C_{66})\}$$

The numerical values are given in Table 2. NdNi intermetallic has a bulk modulus of 60 GPa, i.e. within range of other nickel based binary intermetallics [30]; its magnitude is larger than the calculated value for the ternary $NdNiMg_5$. This can be explained by the larger unit cell volume thanks to the insertion of a light and compressible element Mg with *B* = 45 GPa. On the opposite the trends of shear modules are inverted implying less elasticity of the ternary. As shown in the ELF plots (Fig. 2) Mg brings covalent like bonding besides the metallic bonds of NdNi. Such bonds hinder the gliding of (NdNi) planes with respect to each other. This is further confirmed by the corresponding G_V/B_V ratio which is an indicator of brittleness/ductility: $G/B(NdNiMg_5)$ = 0.51 whereas G/B(NdNi) = 0.39. Knowing that ductile metals have G/B ratios in the range 0.4 – 0.2 [31]; it can be concluded that $NdNiMg_5$ is less

ductile (more brittle) than NdNi. This further confirms the role of the covalent bonding which is discussed hereafter.

4. All electrons non magnetic and magnetic calculations and chemical bonding.

Focusing on $NdNiMg_5$ we now investigate its electronic and magnetic structures as well as the bonding properties. In spite of its experimentally identified antiferromagnetic (AF) ground state [7], the calculations are firstly done for spin degenerate, non spin polarized (NSP), configuration using the experimental crystal data with repeated runs at increasing BZ integration precision. Such a first study allows examining the atom resolved origin of magnetic instability on one hand and permits qualitative description of the chemical bonding based on the overlap populations S_{ij}, on the other hand. Then spin polarized (SP) calculations are done unbiased, i.e. starting from two equal spin populations (↑ and ↓). In fact the SP self consistent computations can lead either to finite magnetization within an implicit long range ferromagnetic order (SP-F) with a stabilization of the energy due to magnetic exchange or to zero magnetization with equal energy to the NSP configuration. Lastly the magnetic ground state, SP-AF is obtained staring from SP-configuration by splitting the unit cell into two magnetic subcells with one as 'UP SPIN' and the other subcell as 'DOWN SPIN'.

Electronic and magnetic structures

At self consistent convergence of the charges and of the (variational) energy, the amount and the sign of charge transfer are similar to the Bader analysis above. The site projected densities of states (PDOS) are displayed in Fig. 3a. The zero energy along the *x* axis is taken with respect to the Fermi energy (E_F). The valence band (VB) is characterized by Ni *d* states centered at -2 eV and Nd 4*f* states lying in E_F. Low intensity states are smeared over the VB as well as above E_F within the conduction band (CB). This is made more explicit Fig. 3b where a narrower *y*-axis range shows the Nd and Ni *p,d* projected PDOS and the total Mg PDOS at the three structure sites. The broad and dispersed Mg states are observed with small differences between them as well as with Nd and Ni on one hand and between Nd and Ni on the other hand; see for instance the resembling Nd and Ni PDOS for a peak at -2 eV at which the Mg1 PDOS equally shows similar skyline PDOS. These observations allow casting a preliminary chemical bonding proposition involving metals *p,d* states with Mg1 *s,p* . This is developed upon in next section. The large DOS's at E_F signal a magnetic instability within the Stoner theory of band ferromagnetism [32]. This is uniquely due to Nd *f* states, i.e. excluding

Ni whose *d*-sates lie completely within the VB. However if a magnetic moment develops on Ni, it will be of induced nature due to the Nd-Ni valence states quantum mixing.

Subsequent SP calculation actually lead to a large energy gain within an implicit ferromagnetic state with ΔE(SP-NSP) = -4 eV/FU. The spin only magnetic moments are then in Bohr magnetons (μ_B): M(Nd) = 3.15; M(Ni)= -0.052; M(Mg1)=0.025; M(Mg2)= -0.006; M(Mg3) = 0.011; M(FU)= 3.22. As expected from the NSP PDOS discussion, only Nd carries a proper magnetic moment whose magnitude approaches the effective moment value of 3.89 μ_B on the contrary Ni has a small magnitude induced moment (negative sign). Also Mg's at the three sites carry small moments due to the bonding with the metal substructures. The site and spin projected DOS shown in Fig. 3c further illustrate these results by the large splitting between ↑ and ↓ Nd PDOS and the small shift between ↑ and ↓ Ni PDOS.

By enforcing SP-AF configuration as detailed above, the energy slightly decreases with respect to SP-F (~-1 eV/FU) which would suggest that the two configurations are close as interpreted on the basis of the small T_N value of 12K [7]. The moment on Nd is then 3.37 μ_B closer to the effective moment value. The full compensation between the SPIN UP and SPIN DOWN magnetic subcells is illustrated in Fig. 3d.

Chemical bonding

The detailed PDOS panel in Fig. 3b clearly shows resembling PDOS between different species of the same chemical nature (Nd, Ni, Mg1, Mg2, Mg3) as well as for species with different chemical natures thus pointing to the bonding between them. Such bonding is rationalized here based on the overlap matrix S_{ij} elements within the COOP scheme [23]. For the first kind of interactions, Fig. 4a shows within the valence band low magnitude COOP for the different interactions, mainly Nd-Nd and Ni-Ni are weakest while there is non-negligible positive COOP (bonding) for Mg2-Mg2 and less for Mg1-Mg1 which show some negative antibonding COOP likely because of their involvement with the interaction with neighboring Nd, Ni and as well as Mg belonging to the other sites. Then the bonding between species of the same kind is not significant for the overall cohesion of the structure except for Mg. Fig. 4b shows the COOP for the interaction between the different Mg substructures. They are more intense and show positive bonding COOP magnitudes. This clearly shows the contribution of Mg to the added cohesion of the compound with respect to NdNi.

Regarding Nd-Ni bonding, we compare it with NdNi intermetallic (insert) in Fig. 4c showing lower magnitude of the Nd-Ni bonding in the ternary. In as far as the Nd-Ni distance is slightly smaller in the ternary (cf. Table 1), which should lead to reinforced Nd-Ni bonding, the argumentation cannot be based on distance consideration. It can be rather argued that the bonding of Nd and Ni with Mg susbstructures should be at the origin of this feature. Fig. 4d shows such bonding exemplified for Mg1 and Mg2 substructures. Actually Mg3 sublattice contributes very small COOP. Indeed the major contributions arise from Nd-Mg1 and Ni-Mg1 which are of bonding nature throughout the VB and NiMg2 which shows bonding and antibonding (negative COOP in 1 eV range below E_F). The positions of the COOP peaks corresponds with the PDOS (Fig. 3), mainly for Ni at the d PDOS peak at ~-2 eV but also with a small contribution from Nd 4*f* at E_F.

5. Conclusions.

In this work the electronic structure of the newly found $NdNiMg_5$ intermetallic compound has been investigated ab initio within DFT. With respect to isostructural NdNi binary large changes brought by Mg have been found as to enhanced cohesive energy, larger compressibility and brittleness. The Mg substructures are found to retain a largely metallic behavior. Summing up on the bonding features, while in NdNi binary the bonding is ensured by Nd-Ni interactions, in the ternary $NdNiMg_5$, Nd-Ni, Nd-Mg, Ni-Mg as well as Mg-Mg participate to the bonding and provide increased cohesion to the crystal lattice as computed in former section thanks to the presence of the extra (Mg) electrons into bonding states.

Acknowledgements

We acknowledge financial support from French-Lebanese CEDRE PHC project, CSR-USEK and CNRS***L***. Support from *Conseil Régional d'Aquitaine*. Computational facilities were provided by MCIA-Université de Bordeaux

References

[1] U. Ch. Rodewald, B. Chevalier, R. Pöttgen. J. Solid State Chem. 180, 1720 (2007).

[2] S. Linsinger, R. Pöttgen, Z. Naturforsch., 66b, 565 (2011).

[3] D. Egusa, E. Abe, Acta Mater. 60, 166 (2012).

[4] S. Couillaud, E. Gaudin, J. L. Bobet, Intermetallics, 19, 336 (2011).

[5] S. Couillaud, E. Gaudin, J. Andrieux, S. Gorsse, M. Gayot, J.L. Bobet, Int. J. Hydrogen Energy, 37, 11824 (2012).

[6] P. Solokha, S. De Negri, V. Pavlyuka, A. Saccone, B.J. Marciniak, J. Solid State Chem., 180, 3066 (2007).

[7] B. Ourane, E.Gaudin, R. Zouari, S. Couillaud, J.-L. Bobet. Inorganic Chemistry 52, 13289 (2013).

[8] S.F. Matar, B. Chevalier, R. Pöttgen. Intermetallics 31, 88 (2012).

[9] W. Kohn, L.J. Sham, Phys. Rev. A, 140 1133 (1964).

[10] P. Hohenberg, W. Kohn, Phys. Rev. B, 136, 864 (1965).

[11] G. Kresse, J. Furthmüller, Phys. Rev. B 54, 11169 (1996).

[12] G. Kresse, J. Joubert, Phys. Rev. B 59, 1758 (1999).

[13] P. E. Blöchl, Phys. Rev. B 50, 17953 (1994) and Phys. Rev. B 49, 16223 (1994).

[14] J. Perdew, K. Burke, M. Ernzerhof, Phys. Rev. Lett. 77, 3865 (1996).

[15] W.H. Press, B.P. Flannery, S.A. Teukolsky, W.T. Vetterling, Numerical Recipes, Cambridge University Press, New York (1986).

[16] M. Methfessel, A. T. Paxton, Phys. Rev. B 40, 3616 (1989).

[17] H.J. Monkhorst, J.D. Pack, Phys. Rev. B, 13, 5188 (1976).

[18] A. D. Becke, K. E. Edgecombe, J. Chem. Phys. 1990,92, 5397; and Nature 1994, 371, 683.

[19] R. Bader. Chem. Rev. 91, 893 (1991).

[20] A.R. Williams, J. Kübler, C.D. Gelatt Jr., Phys. Rev. B 19, 6094 (1979).

[21] V. Eyert, Int. J. Quantum Chem., 77, 1007 (2000).

[22] V. Eyert, The Augmented Spherical Wave Method, Lect. Notes Phys. 849 (Springer, Berlin 2013).

[23] S. F. Matar, J. F. Riecken, B. Chevalier, R. Pöttgen, A. F. Al Alam, V. Eyert, Phys. Rev. B 76, 174434 (2007).

[24] S. Tencé, G. André, E. Gaudin, P. Bonville, A.F. Al Alam, S. Matar, W. Hermes, R. Pöttgen, B. Chevalier. J. Appl. Phys. 106, 033910 (2009).

[25] V. I. Anisimov, J. Zaanen, O.K. Andersen, Phys. Rev. B 44, 943 (1991).

[26] R. Hoffmann, Angew. Chem. Int. Ed. Engl., 26, 846 (1987).

[27 L. Zeng, H. F. Franzen, J. Alloys Compounds, 311, 226 (2000).

[28] S.F. Matar. Matériaux ultra-durs: Concepts et Modélisations. Série Techniques de l'ingénieur. T. I. Sciences et Techniques, Paris (2009) AF 6630 (20pp.)

[29]. O. Beckstein, J.E. Klepeis, G.L.W. Hart, O. Pankratov, Phys. Rev. B 63 (2001) 134112.

[30] S.F. Matar Solid State Sciences, 12, 59, (2010).

[31]. S. Kamran, K. Chen, L. Chen, L. Zhao J. Phys. Condens. Matter, 20, 085221 (2008),

[32] P. Mohn, Magnetism in the solid state – An introduction, springer series, in:

Solid-State Sciences. Springer, Heidelberg, 2003.

Table 1. Experimental and calculated lattice parameters of $NdNiMg_5$ and NdNi. Lattice constants and distances are in units of Å.

$NdNiMg_5$ *Cmcm*, *Z* = 4 FU	Exp. [7]	Calc. (this work)
a	4.4799	4.4687
b	9.9827	10.0085
c	13.7854	13.7389
V /Å ^{37}	616.5	614.47
Nd (4*c*)	½, 0.10948, ¼	½, 0.110, ¼
Ni (4*c*)	0, 0.3254, ¼	0, 0.325, ¼
Mg1 (8*f*)	½,0.40310,0.14140	½, 0.403, 0.141
Mg2 (8*f*)	0,0.20670, 0.07662	0, 0.207, 0.076
Mg3 (4*b*)	½, 0, 0	½, 0, 0
d(Nd-Ni) d(Nd-Mg1) d(Nd-Mg2) d(Ni-Mg2)	2.836 3.291 3.417 2.668	2.86 3.29 3.40 2.67
Energy (eV) / 2FU		–37.61

NdNi *Cmcm*, *Z* = 4 FU	Exp. [24]	Calc. (this work)
a	3.8059	3.8368
b	10.462	10.5599
c	4.3345	4.3563
V /Å ^{3}	172.59	176.50
Nd (4*c*)	0, 0.1385, ¼	0, 0.138, ¼
Ni (4*c*)	0, 0.4273, ¼	0, 0.428, ¼
d(Nd-Ni)	2.916	2.93
Energy (eV)/ 2 FU		–21.98

Table 2 :Calculated elastic properties (in GPa units) of $NdNiMg_5$ and NdNi

	$NdNiMg_5$	**NdNi**
C_{ij}		
C_{11}	79.7	78.4
C_{22}	88.7	81.7
C_{33}	68.4	88.4
C_{44}	27.9	22.4
C_{55}	26.6	33.3
C_{66}	52.8	28.3
C_{12}	45.3	38.1
C_{23}	34.3	59.7
C_{13}	51.7	45.4
Stability combinations		
$C_{11} + C_{22} - 2C_{12}$	+77.8	+83.9
$C_{11} + C_{33} - 2C_{13}$	+44.7	+76.1
$C_{22} + C_{33} - 2C_{23}$	+88.5	+50.7
Bulk (*B*) and Shear (*G*) modules		
B (GPa)	55.5	60.3
G (GPa)	28.5	23.7
G/B	0.51	0.39

Figures captions.

Fig. 1 : Sketch of the $NdNiMg_5$ structure with a projection onto *b,c* plane showing the succession of *NdNi* and Mg layers.

Fig.2 Electron localization function (ELF) slice crossing all chemical species

Fig. 3 $NdNiMg_5$, site a) and b) and spin projected d) and e) DOS.

Fig. 4 $NdNiMg_5$, chemical bonding for the different interactions from COOP criterion.

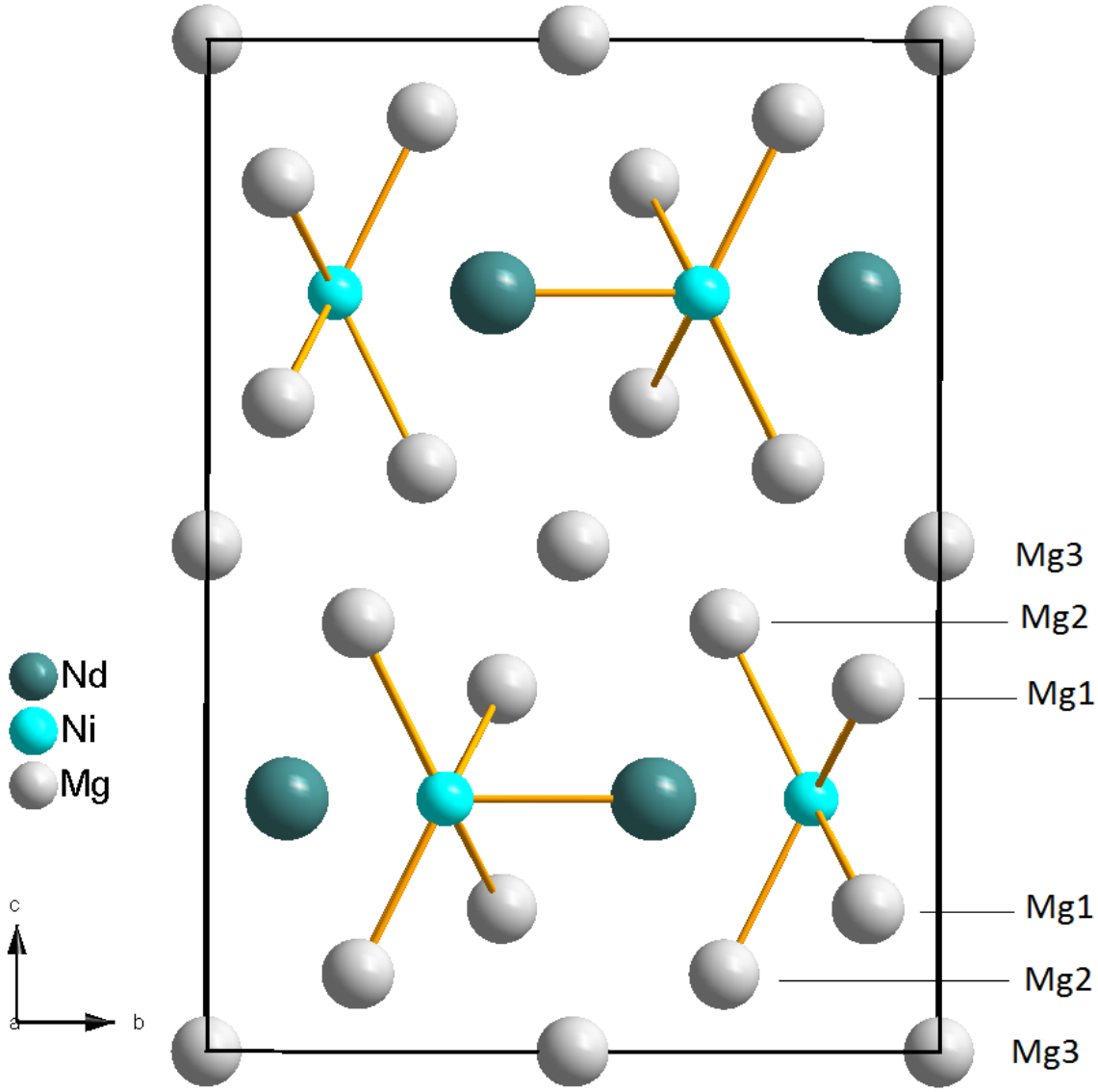

Fig. 1

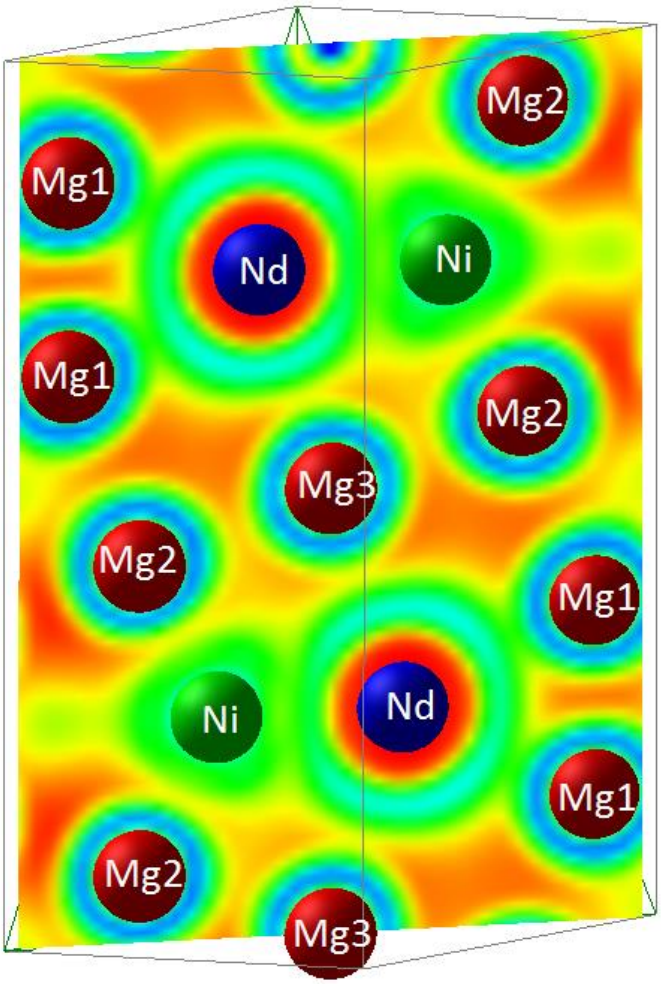

a) $NdNiMg_5$

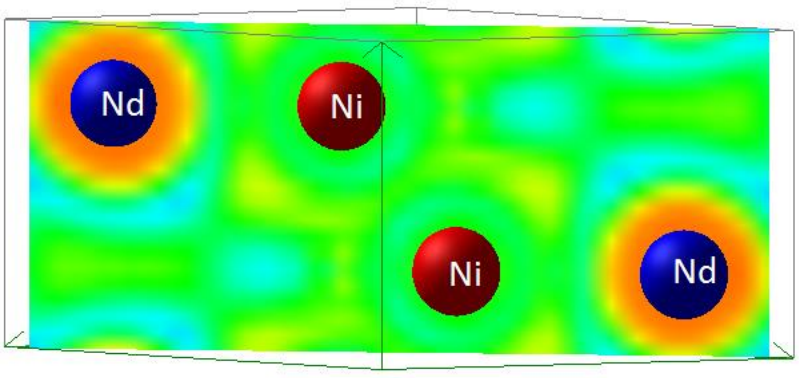

b)NdNi

Fig. 2

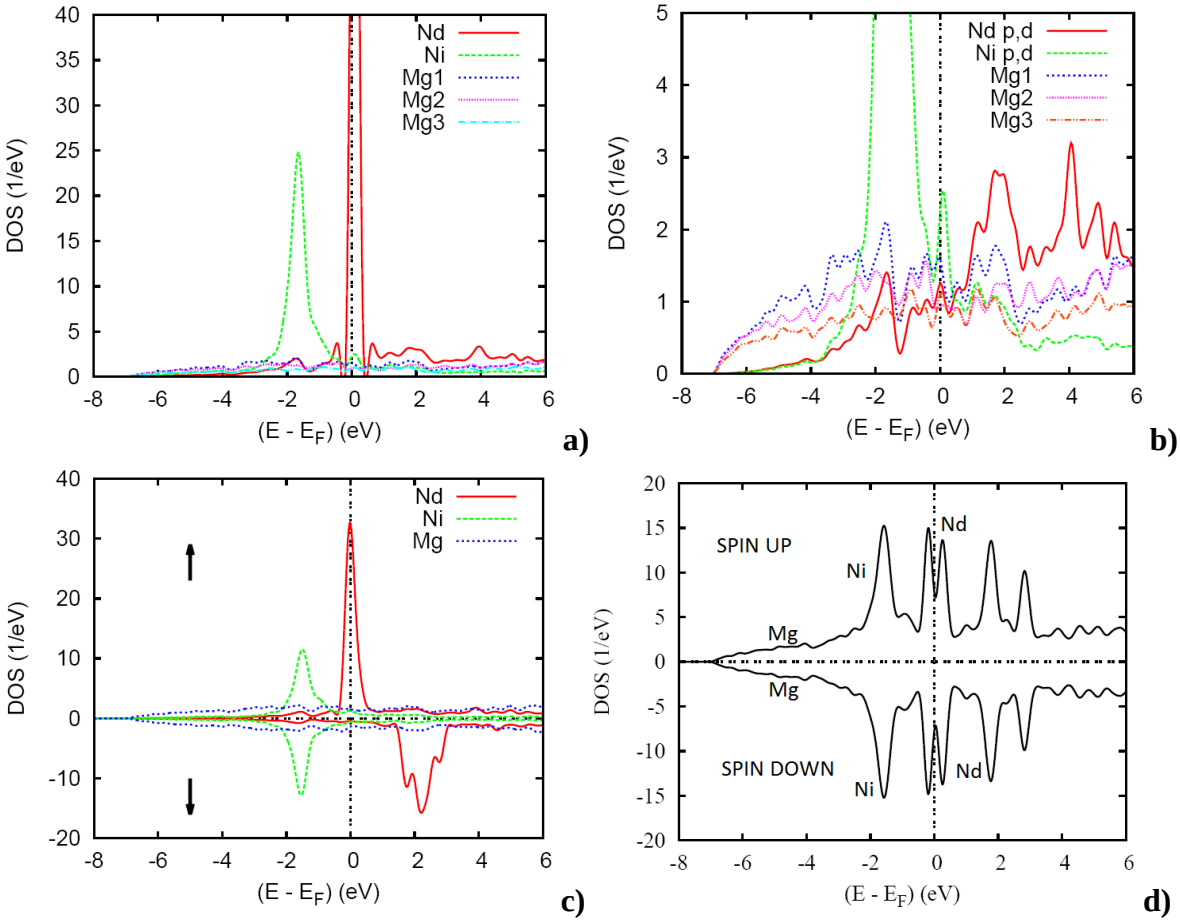
DOS (1/eV)
(E - E$_F$) (eV)
Nd
Ni
Mg1
Mg2
Mg3
a)
Nd p,d
Ni p,d
b)
Mg
c)
SPIN UP
SPIN DOWN
d)

Fig. 3

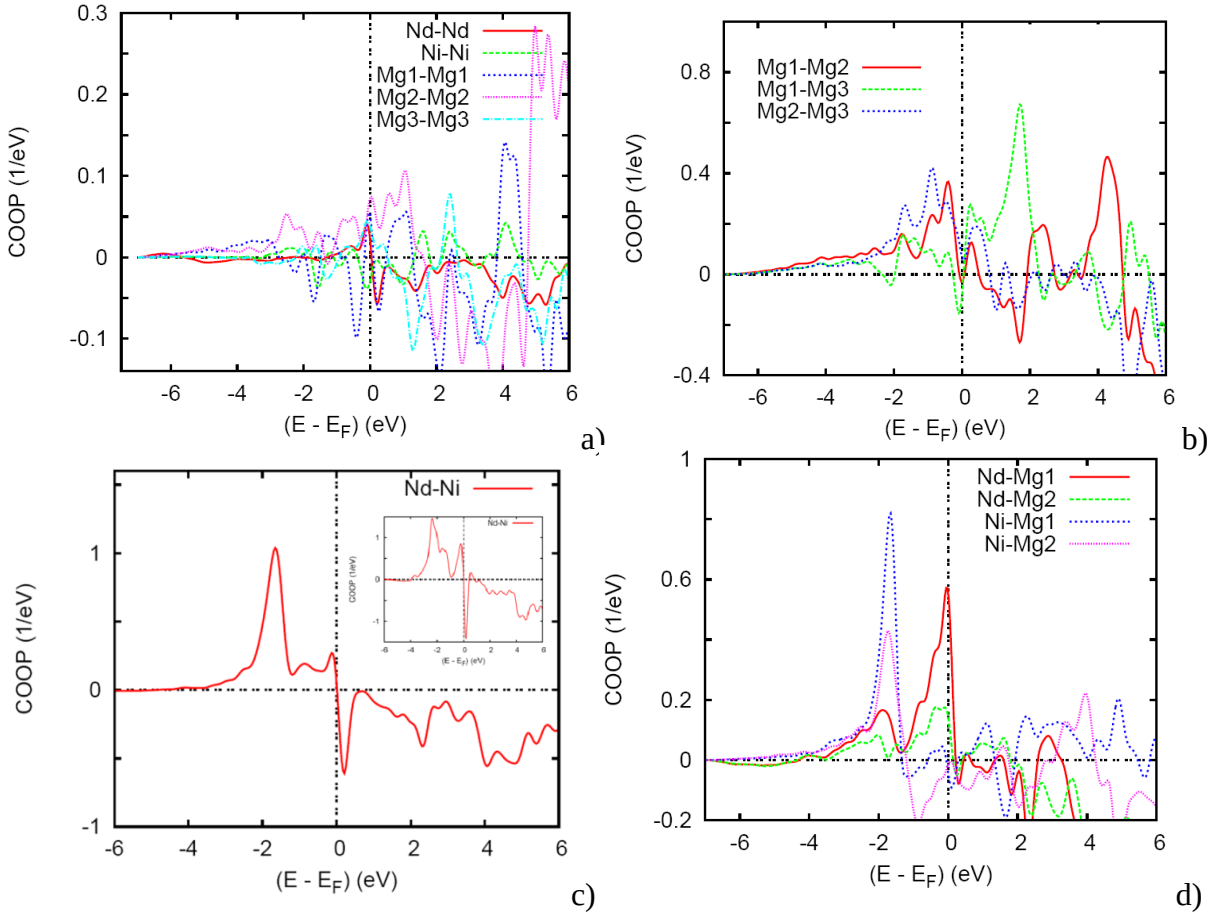
Nd-Nd
Ni-Ni
Mg1-Mg1
Mg2-Mg2
Mg3-Mg3
COOP (1/eV)
(E - E$_F$) (eV)
a)
Mg1-Mg2
Mg1-Mg3
Mg2-Mg3
COOP (1/eV)
(E - E$_F$) (eV)
b)
Nd-Ni
COOP (1/eV)
(E - E$_F$) (eV)
c)
Nd-Mg1
Nd-Mg2
Ni-Mg1
Ni-Mg2
COOP (1/eV)
(E - E$_F$) (eV)
d)

Fig. 4